

ORIGINAL ARTICLE

An all-optical modulator based on a stereo graphene–microfiber structure

Jin-Hui Chen, Bi-Cai Zheng, Guang-Hao Shao, Shi-Jun Ge, Fei Xu and Yan-Qing Lu

An in-line, all-optical fiber modulator based on a stereo graphene–microfiber structure (GMF) utilizing the lab-on-rod technique was demonstrated in this study. Owing to its unique spring-like geometry, an ultra-long GMF interaction can be achieved, and a modulation depth of ~ 7.5 dB (~ 2.5 dB) and a modulation efficiency of ~ 0.2 dB mW^{-1} (~ 0.07 dB mW^{-1}) were demonstrated for two polarization states. The modulation depth and modulation efficiency are more than one order of magnitude larger than those of other graphene–microfiber hybrid all-optical modulators, although at the cost of a higher insertion loss. By further optimizing the transferring and cleaning process, the upper limit of the modulation depth is mainly determined by the loss from the intrinsic absorption, which depends on the light–graphene interaction. Then, the modulator can quickly switch between the on-state and the off-state with a theoretically maximized modulation depth of tens of decibels. This modulator is compatible with the current fiber-optic communication systems and may be applied in the near future to meet the impending need for ultrafast optical signal processing.

Light: Science & Applications (2015) 4, e360; doi:10.1038/lisa.2015.133; published online 4 December 2015

Keywords: graphene; microfiber; optical modulation; polarization

INTRODUCTION

Two-dimensional materials, especially graphene, have attracted global interest¹, and many extraordinary electrical, mechanical, and optical properties have been reported. Regarding their exceptional optical properties, for example, 2.3% linear absorption (related to the fine structure constant)², saturable absorption, and a tunable Fermi level (either by electrical gating^{3,4}, chemical doping^{5,6}, or even plasmon-induced doping⁷) have been demonstrated for a number of broadband optical devices based on graphene in both normal-incidence and waveguide-integrated configurations, such as mode-locked lasers⁸, ultrafast photodetectors^{9–11}, and modulators^{12,13}. Among these, the optical modulator is a key device for optical communication that converts optical or electrical data into optical signals. A high modulation speed, sufficient modulation depth, and large optical bandwidth are indispensable for an optical modulator. Although tuning the Fermi energy by using electric gating on graphene to achieve modulators of gigahertz-level modulation speed has been demonstrated^{12,13}, it is difficult to further improve on the modulation speed due to limitations of the response time of the bias circuit. All-optical modulation can overcome the limitations on the modulation rate by using one light beam to control the transmission of another light beam. This type of modulation may avoid electrical-optical-electrical conversions, thereby rendering the modulation process faster and less noisy. Several papers have reported all-optical modulation schemes with a high speed of 200 GHz based on graphene–microfiber-integrated devices by covering or wrapping a graphene sheet on a straight microfiber. The modulation depth or modulation efficiency is relatively low because a relatively low insertion loss is desirable in these schemes^{14,15}. Higher modulation depth or modulation

efficiency can be achieved with a higher loss by enhancing the light–graphene interaction because of the trade-off among the modulation depth (modulation efficiency), the insertion loss and even the light traveling time. Moreover, it is challenging to handle such a thin microfiber directly for graphene integration with a sufficient length and strength of interaction for practical applications.

Recently, based on the rod-wrapping technique¹⁶, we developed a reliable approach to fabricating graphene–microfiber structure (GMF)-integrated devices by wrapping a microfiber on a graphene-modified rod. This method is much simpler than the conventional integration techniques because we only need to coat a small piece of graphene on a thick rod, rather than a thin microfiber. Theoretically, with a strong evanescent field, the GMF interaction length can be arbitrarily increased using a spring shape of as many turns as is spatially possible. Owing to the extremely asymmetrical cross section of such a stereo GMF device and the nature of the graphene–light interaction¹², different types of losses occur in the two fundamental modes in this hybrid structure. A broadband polarizer can be naturally integrated into such a device¹⁷. The electric fields of the fundamental modes are parallel and vertical to the surface of the supporting rod. In the present study, we show that the stereo GMF structure can also operate as a polarization-dependent, all-optical graphene modulator at approximately 1550 nm, with a very high modulation depth (~ 7.5 dB) and high modulation efficiency (~ 0.2 dB mW^{-1}), which are more than one order of magnitude larger than those reported previously¹⁵. In fact, the modulation depth can be increased to tens of decibels if we can fabricate pure and clean GMF devices by improving the transferring and cleaning process. This type of fiber-integrated,

in-line, all-optical modulator has great potential in fiber optical communication, in which there are demands for high-speed, wideband, low-cost, and integrated methods to modulate information.

MATERIALS AND METHODS

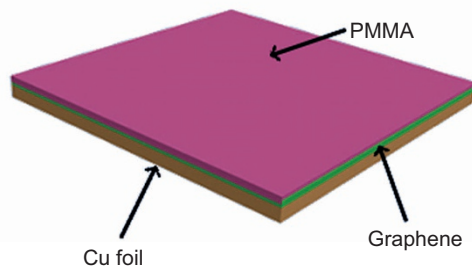
Figure 1 shows the fabrication process of the stereo GMF device. To prevent the loss induced by the relatively high index of the rod (poly-methyl methacrylate or PMMA of diameter ~ 2 mm), a thin low-index Teflon layer (Teflon AF 601S1-100-6, DuPont, tens of micrometers in thickness with a refractive index of ~ 1.31) was dip-coated on the rod's surface and dried in air for several hours. The graphene on the Cu foil (Six Carbon Technology) was first spin-coated with a 4% PMMA-anisole solution and then dried in an oven for 30 minutes at 60 °C. After dissolving the Cu foil using aqueous FeCl_3 at 1 mol L^{-1} and cleaning the sample in deionized water (DI), the PMMA/graphene film was removed from the DI water using a rod. The surface tension led to the film tightly encapsulating the rod when the film left the DI water. Then, the rod with the graphene/PMMA film was heated in an oven for 30 minutes at 80 °C, and the PMMA film was removed by acetone. Finally, a tapered microfiber was wrapped onto the graphene-functionalized rod.

Raman spectroscopy was carried out by using the 488 nm (2.54 eV) lines of an Ar ion laser as excitation sources. The laser beam was focused onto the sample using a $50\times$ microscope objective lens (0.8 N.A.), and the scattered light was analyzed by a monochromator. The Raman spectrum clearly shows the single-layer nature of the transferred graphene¹⁸, as shown in Figure 2. In our experiment, we chose a microfiber with a diameter of $\sim 3 \mu\text{m}$, and there were two microfiber coils on a rod, which implies that the light–graphene interaction

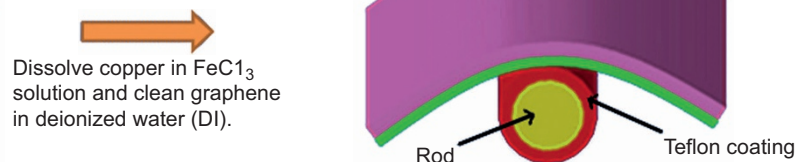
length was $\sim 12 \text{ mm}$. The microfiber in our experiment was tapered from a conventional single mode fiber by utilizing a flame-brushing technique.

The all-optical modulation mechanism is based on the Pauli blocking effect, as illustrated in Figure 3a. When a high-power pump light at a short wavelength excites dense carriers in graphene from the valence band to the conduction band, the non-equilibrium carrier distribution broadens and equilibrates with the intrinsic carrier population through carrier–carrier scattering. The scattering process lasts for only hundreds of femtoseconds. The subsequent cooling and decay of the hot distribution through carrier–phonon scattering occur on a time scale of picoseconds¹⁹. Carriers relaxing from the conduction band leads to a band-filling effect, which results in a significant reduction in the graphene absorption for light of a greater wavelength. In this manner, we can use a high-power pump light source to switch a weak probe light source. As we can see above, the photon-excited carrier's relaxation process is dominated by carrier–phonon scattering, which lasts for several picoseconds. In other words, the all-optical modulation speed can theoretically reach hundreds of gigahertz. This has been experimentally demonstrated by using ultrafast optical pump-probe spectroscopy to measure the decay time of graphene carriers coated on a straight microfiber¹⁴. Moreover, the modulation depth increases with the light–graphene interaction length and strength, which are greatly enhanced in the stereo GMF platform. However, inhomogeneous interaction in the large-length, light–graphene interaction inevitably leads to an inhomogeneous graphene response and thus limits its fast response. As a result, a trade-off should exist between the modulation depth and response time, as discussed below.

1. PMMA on graphene grown on copper foil



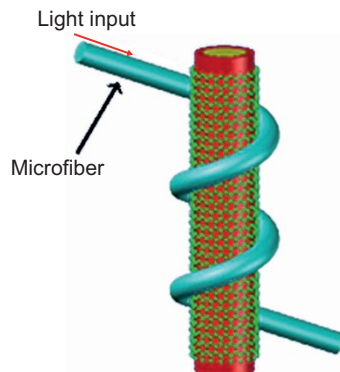
2. Graphene on PMMA film wrapped onto supporting rod



Dissolve copper in FeCl_3 solution and clean graphene in deionized water (DI).

Remove the PMMA/graphene film from DI water using a rod. Dry the sample in an oven and dissolve the PMMA film in acetone.

4. GMF schematic structure



3. Graphene on rod

Taper a microfiber and wrap it onto the graphene-coated rod



Figure 1 Fabrication process of the stereo hybrid GMF device. Panels 1–3 demonstrate the detailed steps for transferring graphene onto a rod. Panel 4 shows a schematic structure of the GMF device.

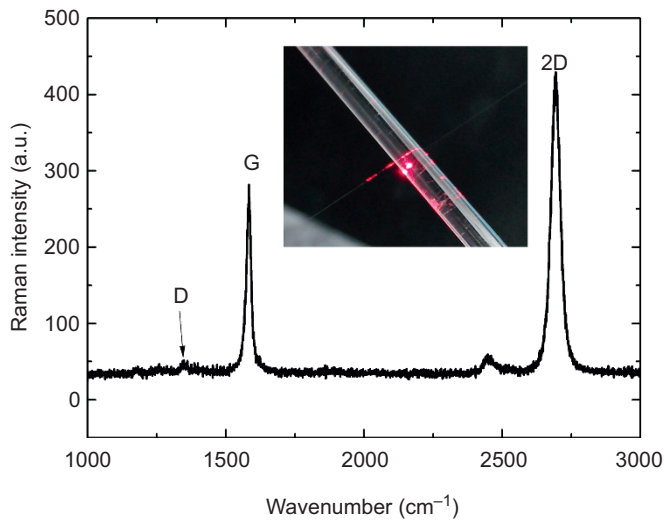


Figure 2 Raman spectrum of a monolayer graphene film. Inset, camera image of the as-fabricated GMF device, launched with a 650 nm light source. The strong scattering region indicates the graphene–microfiber interaction region.

RESULTS AND DISCUSSION

In our experiment, we first used a continuous-wave (CW) pump light source at 980 nm (OPEAK, Pump-LSB-980-500-SM) to measure the static modulation characteristics of our polarization-dependent stereo GMF platform, as shown in Figure 3b. Here, we call it “static” to distinguish it from the later pulse pump probe experiment, which is called “dynamic”. Because the amplified spontaneous emission (ASE) light source (Connet C-ASE Optical Source) is non-polarized, a linear polarizer and a half-wave plate are incorporated between the light source and fiber wavelength-division multiplexer (WDM) to selectively excite different eigen-modes of our GMF with the same launching power. The ASE power input in our experiment was fixed at $\sim 300 \mu\text{W}$. As shown in Figure 3c, when the pump light is switched off, the output intensity difference between the low absorption-loss mode (LAM) and the high absorption-loss mode (HAM) is approximately 15 dB at 1550 nm, which is attributable to the broken symmetry of the GMF geometry and the absorption nature of graphene. The difference can be reduced or even eliminated by increasing the pump power. The small ripple superposed in the output spectra is attributable to the interface interference caused by the polarizer.

As the pump power increases, the output intensities of the HAM and LAM also increase because of the saturable absorption properties of graphene, as shown in Figure 3c. Here, we define the modulation depth as the transmission change of one polarization mode in the

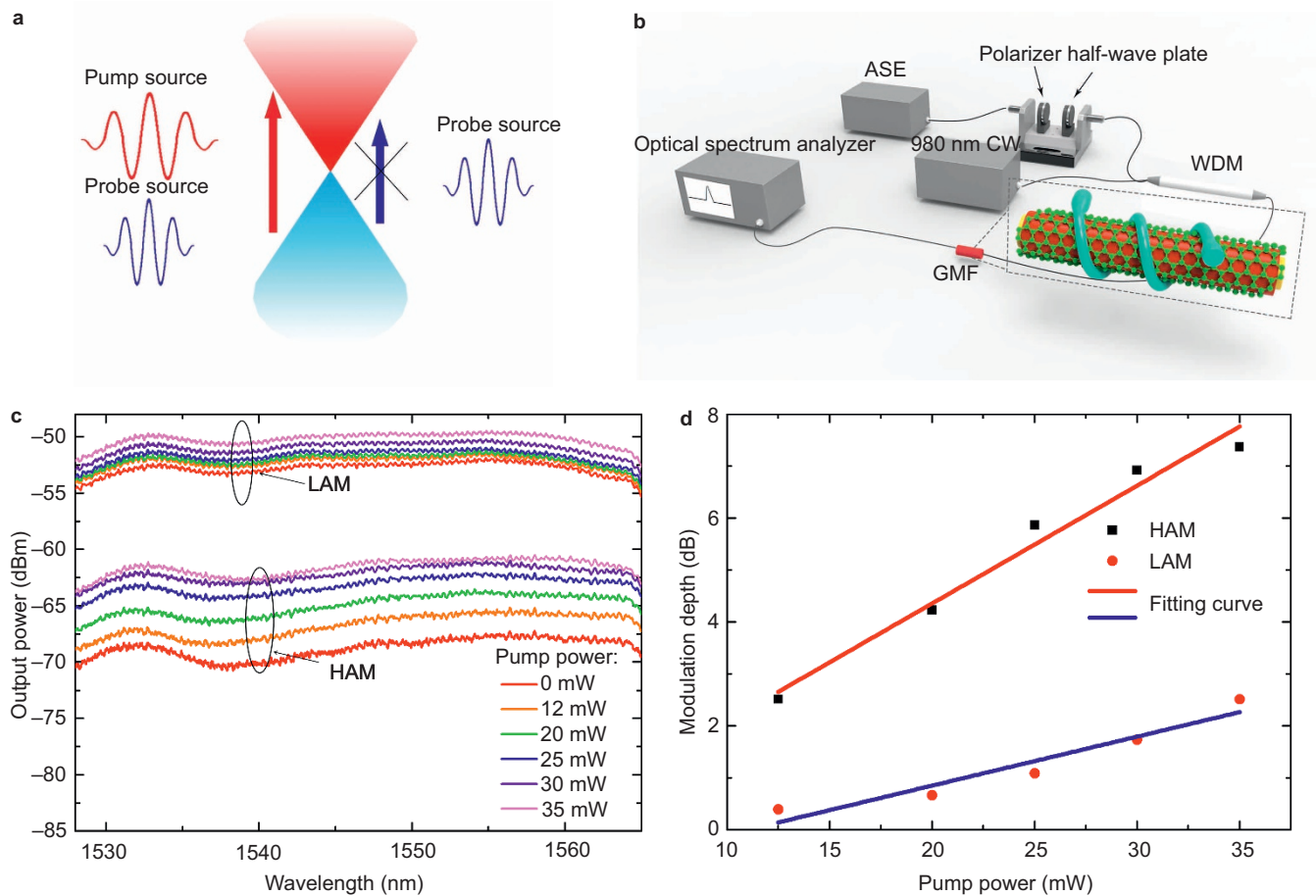


Figure 3 CW-pump-based modulation measurement system and results. (a) Schematic illustration of the all-optical modulation mechanism. (b) CW pump probe measurement system. (c) Output spectra of the stereo GMF device with a 980-nm pump source with different powers for the LAM and HAM. (d) Changes in modulation depth with different pump powers for 1550-nm probe wavelength, extracted from (c). The blue and red lines are numerical fitting curves.

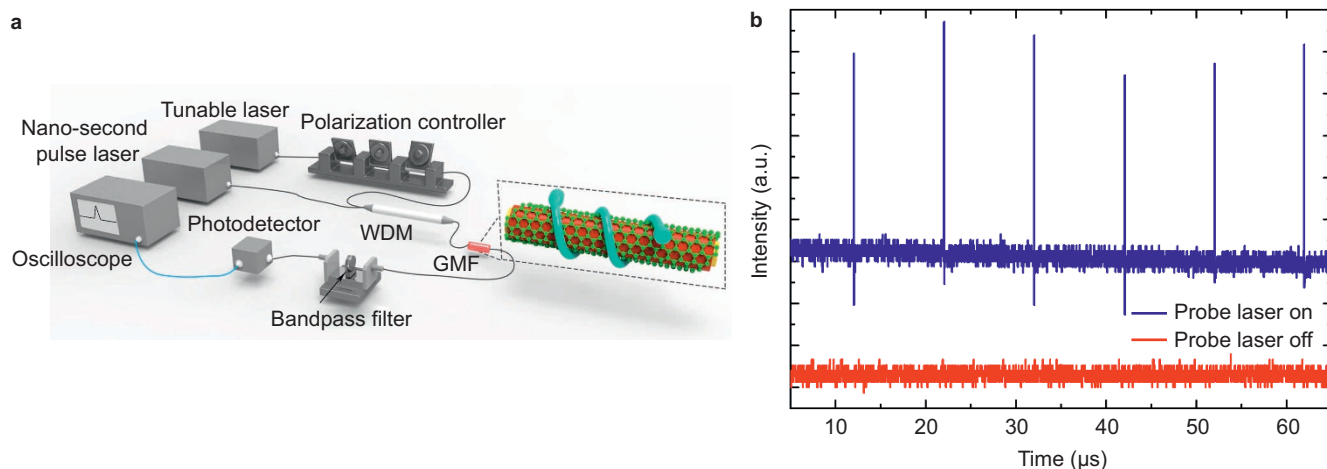


Figure 4 Pulse-laser pump probe system. (a) Optical measurement system. (b) Time-domain response of the GMF modulator. The modulated probe light curve was moved up for clarity.

GMF device. The modulation efficiency is the modulation depth of the GMF device per unit pump power. In Figure 3c, when the pump power reaches 35 mW, the modulation depths of the HAM and LAM are 7.5 dB and 2.5 dB, respectively, in the range of 1525–1565 nm. Accordingly, the modulation efficiencies of the HAM and LAM are $\sim 0.2 \text{ dB mW}^{-1}$ and $\sim 0.07 \text{ dB mW}^{-1}$, respectively. The polarization-dependent characteristics can provide more options, and we can achieve different modulation depths (insertion losses) for different polarization states, depending on the specific requirements of the practical application. Moreover, we can use an in-line fiber polarizer to select the desired launched polarization of light and thereby avoid the extra noise caused by polarization mixing. In Figure 3d, we can see that the modulation depth of the GMF increases linearly with the pump power. To further illustrate the relation between the modulation depth and the pump power, we build a classical small-signal amplification model²⁰ to fit the experimental data (see Supplementary Information Note 1). It should be noted that the linear relation between the modulation depth and the pump power holds only for the small-signal condition. As the modulation depth increases with the pump power, it will reach a saturation value, and the linear relation will naturally break down. In our numerical calculation, the theoretical maximum modulation depth of our platform is $\sim 23 \text{ dB}$ and 5.4 dB for the HAM and LAM, respectively (see Supplementary Information Note 2), for a $3.0\text{-}\mu\text{m}$ -diameter microfiber with a two-coil structure. For a $2.5\text{-}\mu\text{m}$ -diameter microfiber, the modulation depths of the HAM and LAM should be 42 dB and 9.6 dB ($L \sim 12 \text{ mm}$), respectively. The modulation depth can be further improved if we optimize the coil number and microfiber diameter. Then the HAM can switch between the on-state and the off-state with an exceptionally large contrast, a fast speed and an unavoidable insertion loss from the intrinsic absorption.

As we can see, our current experimental results only reach one-third of the theoretical values at a $3.0 \mu\text{m}$ diameter. One of the reasons is that the maximized pump power we used did not saturate over the entire GMF interaction length. The reason why we did not further increase the pump power in our experiment was that breakdown power threshold of the GMF existed because many residues of the protecting film of PMMA remained on the graphene surface after the PMMA removal process, which caused a great heating effect when launched with a high pump power. The average insertion losses for HAM and LAM are $\sim 10 \text{ dB/turn}$ and $\sim 5 \text{ dB/turn}$, respectively, in our experiments, which are larger than the simulation results (Supplementary Information Note 2). We

attribute this to the contamination of the graphene during the transfer process. If the fabrication method is perfected (for example, the PMMA can be fully removed, and only pure graphene will be left), the modulation depth of our GMF can be further improved to approach the theoretical value, which is mainly determined by the insertion loss from the intrinsic absorption. The higher modulation depth upper-limit always entails a higher insertion loss that depends on the light–graphene interactions. In practical applications, we must balance the interaction length between the insertion loss and the modulation depth based on real requirements.

To observe the time-domain response of the GMF modulator, we used a nanosecond laser (KEOPSYS, PYFL-K04-RP-030-006-050-1064-T0-ET1-PK5D-FA) at 1064 nm to conduct the pump probe experiment. The pump probe system is illustrated in Figure 4a. We used a bandpass filter centered at 1550 nm with a full width at half maximum (FWHM) of 12 nm to filter out the pump pulse laser. The modulated probe light was then detected by a photo-detector (New Focus, 1544-B), and the transformed electric signal could be analyzed by an oscilloscope (Agilent Technologies, DSO-X 4024A). When the pulse laser (pulse width of $\sim 6 \text{ ns}$, repetition rate of 100 kHz) of average power 1.5 mW was launched into the GMF device along with a CW 1550-nm probe light (Agilent, tunable laser 81980 A) of power $\sim 5 \text{ mW}$, the pulse laser increased the probe light transmission of the GMF device in their presence and switched off the probe source when they were absent. This can be readily seen in Figure 4b. When the probe laser was switched off, there was no modulated serial signal, which reflects the excellent filtering of the pump light. When the probe laser was turned on, a modulated probe light was clearly observed, which unambiguously demonstrated that our GMF device could serve as an all-optical modulator. Although we only demonstrated 100-kHz modulation repetition, the GMF structure can be operated at sub-THz repetition rates for the ultrafast carrier relaxation of graphene¹⁴.

There is concern that the longer light–graphene interaction length may lead the pump and probe light to separate because of group velocity dispersion, thus limiting the fast response. We think that this problem may be inevitable if a high modulation depth is demanded because there is a balance between the response time and the modulation depth. Of course, there are several methods to ease the contradiction. First, it is convenient to tune the group velocity dispersion of a microfiber by coating a thin film, such as Teflon or polydimethylsiloxane (PDMS), onto the surface of the microfiber²¹. Second, we can choose a thinner

microfiber and a thinner supporting rod to reduce the interaction length while achieving a reasonably good modulation depth.

CONCLUSIONS

Using a GMF-integrated stereo device, we demonstrated a highly polarization-sensitive all-optical modulating platform. The unique geometry practically enabled a sufficient light–graphene interaction length and strength, and a modulation depth of ~ 7.5 dB (~ 2.5 dB) and modulation efficiency of ~ 0.2 dB mW^{-1} (~ 0.07 dB mW^{-1}) were simultaneously achieved for the HAM (LAM). The polarization-dependent modulation characteristics and time-domain response were also investigated. The performance was limited by the relatively low quality of the graphene used in the platform. A modulation depth as high as the theoretical prediction (~ 23 dB at a 3 μm diameter, HAM) can be expected by improving the transfer and wrapping processes of the graphene. The findings of this study may contribute to many future applications in all-optical fiber-optic circuits.

ACKNOWLEDGEMENTS

This work is sponsored by the National 973 program (2012CB921803 and 2011CBA00205), the National Science Fund of China under grants 61225026, 61322503, 61457069, 61435008 and 61490714, and the Fundamental Research Funds for the Central Universities. The authors thank Hao Qian and Song-hua Cai for their assistance in drawing the schemes. The authors also thank the anonymous reviewers for their gracious comments, which helped us improve the paper.

- 1 Novoselov KS, Geim AK, Morozov SV, Jiang D, Zhang Y *et al*. Electric field effect in atomically thin carbon films. *Science* 2004; **306**: 666–669.
- 2 Nair RR, Blake P, Grigorenko AN, Novoselov KS, Booth TJ *et al*. Fine structure constant defines visual transparency of graphene. *Science* 2008; **320**: 1308.
- 3 Li ZQ, Henriksen EA, Jiang Z, Hao Z, Martin MC *et al*. Dirac charge dynamics in graphene by infrared spectroscopy. *Nat Phys* 2008; **4**: 532–535.

- 4 Gan XT, Shiue RJ, Gao YD, Mak KF, Yao XW *et al*. High-contrast electrooptic modulation of a photonic crystal nanocavity by electrical gating of graphene. *Nano Lett* 2013; **13**: 691–696.
- 5 Schedin F, Geim AK, Morozov SV, Hill EW, Blake P *et al*. Detection of individual gas molecules adsorbed on graphene. *Nat Mater* 2007; **6**: 652–655.
- 6 Wehling TO, Novoselov KS, Morozov SV, Vdovin EE, Katsnelson MI *et al*. Molecular doping of graphene. *Nano Lett* 2008; **8**: 173–177.
- 7 Fang ZY, Wang YM, Liu Z, Schlather A, Ajayan PM *et al*. Plasmon-induced doping of graphene. *ACS Nano* 2012; **6**: 10222–10228.
- 8 Bao QL, Zhang H, Wang Y, Ni ZH, Yan YL *et al*. Atomic-layer graphene as a saturable absorber for ultrafast pulsed lasers. *Adv Funct Mater* 2009; **19**: 3077–3083.
- 9 Gan XT, Shiue RJ, Gao YD, Meric I, Heinz TF *et al*. Chip-integrated ultrafast graphene photodetector with high responsivity. *Nat Photonics* 2013; **7**: 883–887.
- 10 Mueller T, Xia FN, Avouris P. Graphene photodetectors for high-speed optical communications. *Nat Photonics* 2010; **4**: 297–301.
- 11 Xia FN, Mueller T, Lin YM, Valdes-Garcia A, Avouris P. Ultrafast graphene photodetector. *Nat Nanotechnol* 2009; **4**: 839–843.
- 12 Liu M, Yin XB, Ulin-Avila E, Geng BS, Zentgraf T *et al*. A graphene-based broadband optical modulator. *Nature* 2011; **474**: 64–67.
- 13 Gao YD, Shiue RJ, Gan XT, Li LZ, Peng C *et al*. High-speed electro-optic modulator integrated with graphene-boron nitride heterostructure and photonic crystal nanocavity. *Nano Lett* 2015; **15**: 2001–2005.
- 14 Li W, Chen BG, Meng C, Fang W, Xiao Y *et al*. Ultrafast all-optical graphene modulator. *Nano Lett* 2014; **14**: 955–959.
- 15 Liu ZB, Feng M, Jiang WS, Xin W, Wang P *et al*. Broadband all-optical modulation using a graphene-covered-microfiber. *Laser Phys Lett* 2013; **10**: 065901.
- 16 Kou JL, Chen Y, Xu F, Lu YQ. Miniaturized broadband highly birefringent device with stereo rod-microfiber-air structure. *Opt Express* 2012; **20**: 28431–28436.
- 17 Kou JL, Chen JH, Chen Y, Xu F, Lu YQ. Platform for enhanced light–graphene interaction length and miniaturizing fiber stereo devices. *Optica* 2014; **1**: 307–310.
- 18 Ferrari AC, Meyer JC, Scardaci V, Casiraghi C, Lazzeri M *et al*. Raman spectrum of graphene and graphene layers. *Phys Rev Lett* 2006; **97**: 187401.
- 19 Dawlaty JM, Shivaraman S, Chandrashekar M, Rana F, Spencer MG. Measurement of ultrafast carrier dynamics in epitaxial graphene. *Appl Phys Lett* 2008; **92**: 042116.
- 20 Yariv A, Yeh P. *Optical Electronics in Modern Communications*. 6th ed. Oxford: Oxford University Press; 2007: 230–232.
- 21 Xu ZY, Li YH, Wang LJ. *In situ* fine tailoring of group velocity dispersion in optical microfibers via nanocoatings. *Opt Express* 2014; **22**: 28338–28345.



This license allows readers to copy, distribute and transmit the Contribution as long as it attributed back to the author. Readers are permitted to alter, transform or build upon the Contribution as long as the resulting work is then distributed under this is a similar license. Readers are not permitted to use the Contribution for commercial purposes. Please read the full license for further details at - <http://creativecommons.org/licenses/by-nc-sa/4.0/>

Supplementary Information for this article can be found on the *Light: Science & Applications*' website (<http://www.nature.com/lsa/>).